J Eng Math (2008) 61:271–284
DOI 10.1007/s10665-007-9209-8

Modelling of residual stresses developed in steel cylinders subjected to surface-layer deposition by welding

Igor K. Senchenkov · Yaroslav A. Zhuk · Olga P. Chervinko · Eugeniusz Turyk

Received: 6 November 2006 / Accepted: 18 December 2007 / Published online: 6 February 2008

Abstract A new model for the determination of the residual stress–strain and microstructural state of a cylinder subjected to layer deposition by welding is developed. The growing body of theory and unified the Bodner–Partom viscoplastic theory generalized for the case of coupled thermomechanic processes are involved to describe the mechanical behavior of the material. Continuous cooling transformation (CCT) diagrams are used to account for microstructural transformation. The concept of eigenstrains and temperature state is utilized to satisfy the boundary conditions on the growing surface. A time-stepping procedure and a finite-element technique are used to simulate both the instantaneous and the residual stress–strain and microstructural state of a deposited cylinder. The influence of initial temperature on the residual stress–strain and the structural states of the cylinder deposited by austenitic and martensitic steel layers is investigated. It is discovered that martensite and bainite shares in the heat-affected zone can be effectively controlled by the initial temperature of the cylinder. Numerical and experimental results are compared.

Keywords Finite-element method · Growing body · Residual stresses · Structure transformation · Thermoviscoplasticity

1 Introduction

The development of thermo-elasticity and thermoplasticity theories as integral parts of general thermomechanics was stimulated by the necessity of analyzing the strength of machine parts [1, Sects. 1–4], determining the rational parameters of processes such as welding and related technologies, and evaluating process-induced residual stresses and strains [2, Chap. 3]. Kovalenko and his followers [3, Chap. 1] and [4, Chaps. 1,2] laid the theoretical foundation for these research areas. The technological advance calls for further research in these areas based on new, often nonclassical approaches.

I. K. Senchenkov (✉) · Y. A. Zhuk · O. P. Chervinko
Timoshenko Institute of Mechanics, National Academy of Sciences of Ukraine, Nesterov Str. 3, Kiev 03057, Ukraine
e-mail: term@inmech.kiev.ua

E. Turyk
The Welding Institute, ul. Bl. Czeslawa 16/18, 44-100 Gliwice, Poland
e-mail: Eugeniusz.Turyk@is.gliwice.pl

Modeling the formation of residual stresses and strains in processes where a material is applied onto the free surface of a body under nonisothermal conditions is an important thermomechanical problem. According to the methods used to simulate such processes, this problem is tackled within the framework of the theory of growing deformable bodies [5, Chaps. 1–3]. Interest in such problems has been revived because of the development of macro- and micro-level processes. The macrolevel processes include building-up, sputtering, and other manufacturing and repair techniques [6, Chaps. 1–3], [7, pp. 24–48], [8, Chaps. 1–4] and [9], all falling into the class of solid free-form fabrication (SFF) processes [10]. The idea underlying such processes is to form a solid body by directly applying a material (a melt as a rule) onto its surface.

A material may be applied either continuously or discretely. SFF-processes are methods to produce inhomogeneous structures such as so-called smart materials and finished articles consisting of (piezo-, etc.) active and passive layers or inclusions [11, pp. 304–368] and [12].

Among microlevel processes is nanotechnology, since one of the basic techniques for producing nanomaterials, in particular composites, is spraying [13,14].

A distinguishing feature of the formulation of thermomechanics problems for growing bodies is that all the components of the stress tensor must be specified on the growth surface [5, Chaps. 1–3], in contrast to the classical formulation where the components of the load vector are specified on the surface. The formulation and solution methods become more involved if the body grows under nonisothermal conditions and its material is physically nonlinear. In this case, thermal and inelastic effects predominate in the formation of transient and residual stress–strain states [3, Chap. 1], [4, Chaps. 1,2].

The physical nonlinearity and temperature dependence of the material properties call for the use of numerical methods. The numerical approaches applied to the problems of build-up and multipass welding are reviewed in [2, Chap. 3] and [15,16]. A specific feature of growing (building-up) processes is that the vector of total displacements discontinues on the growth surface. Therefore, the standard numerical methods, such as the finite-element method (FEM) in Lagrangian formulation, fail here because they assume continuous displacements at the outer nodes of an element [17, Chap. 2]. Such problems are solved within a separate research area, namely the mechanics of media with discontinuous fields including discontinuities at inner boundaries [18,19]. To apply the FEM to such problems, an additional vector of varied variables conjugate to the field of displacement discontinuities is introduced. This results in a governing system of algebraic equations of very high order. The large number of variables affects problems with highly localized and varying field quantities, which requires mesh refinement. In this connection, it is advisable to solve practical problems with the help of properly modified and regularized standard FEM codes. The fundamentals of such an approach, developed for thermo-elastic materials and based on the concept of a natural pre-thermostrained state, are outlined in [20,21].

The further step is presented in paper [22,23] devoted to the modelling of thermomechanical process of roller surfacing by layers of austenite steel. The austenitic steel does not undergo structural transformation during cooling, so that it is possible to ignore the effect at this stage on the residual strain–stress state of the deposited layers. But in practice, it is necessary more often to apply a surface consisting of a layer of the stronger martensitic steel. Under these conditions preheating as well as presurfacing of high plastic austenitic steel layers are utilized to prevent the generation of cracks.

The present work generalizes an approach developed in [22,23] for the case of viscoplastic materials with structure transformation within the Bodner–Partom unified viscoplastic model [21]. The main contribution of the present paper is a new model for determining the residual stress–strain and microstructure (SSMS) state of a cylinder subjected to surface-layer deposition by welding developed on the basis of the growing-body theory [5, Chaps. 1–3] and [23] using the concept of eigenstrains and temperature [20,22,23], unified Bodner–Partom viscoplastic theory [24, Chap. 1] and continuous-cooling transformation (CCT) diagrams [25, Chap. 1] and [26, pp. 12–108]. The change of the structural state of a martensitic component is accounted for by the volume change as well as a change of Bodner–Partom model parameters modified in an appropriate way.

As an example, we will consider a finite cylinder spacially growing on the lateral surfacing.

The paper consists of two conceptual parts. The first is devoted to an investigation of the residual SSMS states of the roller surfacing by austenitic steel layers. In the second part we consider the particulars of the SSMS states

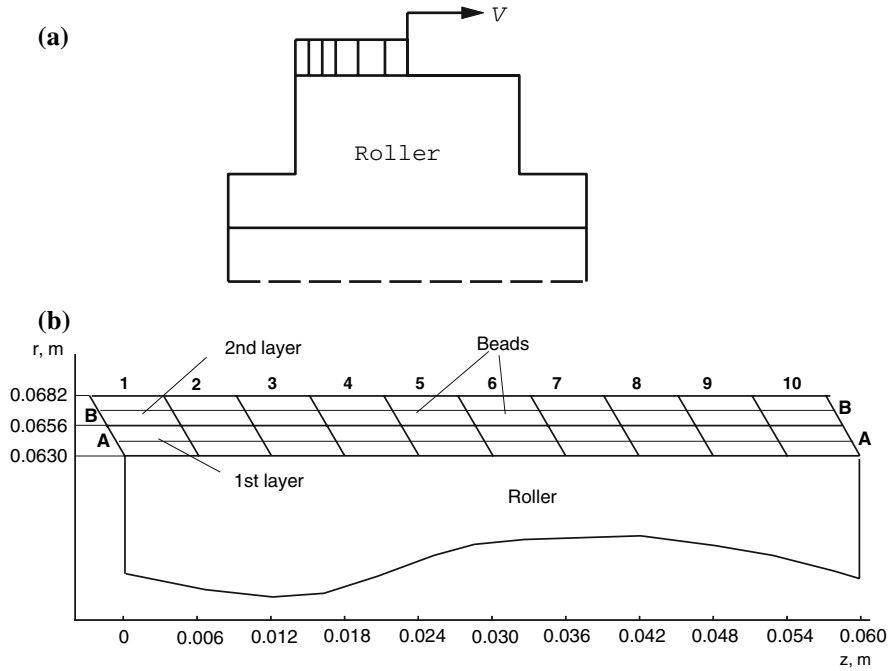

Fig. 1 The diagram of gradual growth of the disposed layer (**a**) and deposition of beads with and without overlapping of the layers (A–A and B–B are the median lines of the first and second deposited layers (**b**))

when a martensitic outer layer is deposited as well as martensitic transformations in the roller material taking place. It is established that the SSMS state of deposited cylinder is effectively controlled by the preset initial temperature of the cylinder.

2 Problem formulation

The cylinder (Fig. 1) is defined in a cylindrical coordinate frame $Orz\varphi$ with $0 < z < L, 0 < r < r_0$. The material is isotropic. The general three-dimensional problem of a spirally growing multilayer cylinder (roller) is considered as axisymmetric, i.e., it is assumed that equivalent circular beads are built up on the outer surface of the cylinder.

Further we take the word "deposition" to mean a sequential filling of initially empty beads with liquid steel. The temperature of the steel is calculated from the welding energy balance.

The beads of the first layer are first deposited from $z = 0$ to $z = L$. The beads are presented in the shape of a parallelogram and are shown by thick lines in Fig. 1b. Then, sequentially the beads of the 2nd layer are deposited, etc.

The formulation of the problem includes the kinematic relations, the heat-conduction equation

$$c_v\dot{\theta} = \operatorname{div}(k \operatorname{grad}\theta) + q_{\text{vol}}, \tag{1}$$

the quasistatic equilibrium equation

$$\operatorname{div}\boldsymbol{\sigma} = 0 \tag{2}$$

and the boundary and initial conditions:

$$\theta = \theta_0 \ \text{ at } \ t = 0; \quad -k\vec{n} \cdot \operatorname{grad}\theta = -q_{\text{ar}} + \gamma(\theta - \theta_C) + \sigma\varepsilon\left(\theta^4 - \theta_0^4\right), \tag{3}$$

$$\boldsymbol{\sigma} \cdot \vec{n} = 0, \tag{4}$$

where θ is the temperature, $\boldsymbol{\sigma}$ is the stress tensor, q_{ar} is the density of the heat flow supplied through the surface, q_{vol} is the volumetric heat-flow density, c_v and k are the coefficients of thermal capacity and thermal conductivity, $\gamma = 30$ W/(m^2 °C) is the heat-transfer factor, $\theta_C = 20$°C is the ambient temperature, θ_0 is the initial temperature, $\vec{n}$ is the outward normal to the body's surface, σ is Stefan's constant, $\sigma = 5.67 \times 10^{-5}$ erg cm^{-2}s^{-1} deg^{-4}; ε is the emissivity factor, and tensor quantities are marked with bold letters ($\boldsymbol{\sigma} = \sigma_{ij}$; $i, j = r, z, \varphi$).

The thermomechanical behavior of the material is described by the modified Bodner–Partom model [24, Chap. 1] and [27]. These papers include the additive representation of total strain and plastic incompressibility rule

$$\boldsymbol{\epsilon} = \boldsymbol{\epsilon}^e + \boldsymbol{\epsilon}^p + \boldsymbol{\epsilon}^{\theta\text{ph}}, \quad \text{tr}\,\boldsymbol{\epsilon}^p = 0, \tag{5}$$

Hooke's constitutive equation

$$\boldsymbol{s} = 2G\left(\boldsymbol{e} - \boldsymbol{\epsilon}^p\right), \quad \text{tr}\,\boldsymbol{\sigma} = 3K_v \text{tr}\left(\boldsymbol{\epsilon} - \boldsymbol{\epsilon}^{\theta\text{ph}}\right), \tag{6}$$

the isotropic form of the Prandtl–Reuss flow law with associated von Mises yield criterion

$$\dot{\boldsymbol{\epsilon}}^p = D_0 \exp\left\{-\frac{1}{2}\left[\frac{\left(\bar{K}_0 + K\right)^2}{3J_2}\right]^n\right\} \frac{\boldsymbol{s}}{J_2^{1/2}}, \quad \boldsymbol{\epsilon}^p(0) = \boldsymbol{0}, \tag{7}$$

the evolution equation for isotropic hardening

$$\dot{K} = m_1\left(\bar{K}_1 - K\right)\dot{w}_p, \quad K(0) = 0, \tag{8}$$

where G, G_f and K_V, K_{Vf} are shear and bulk moduli; $\bar{K}_0$ and $\bar{K}_1$ are calculated by the formulae $\bar{K}_0 = C^\xi K_0^\xi$, $\bar{K}_1 = C^\xi K_1^\xi$; C^ξ denotes bulk concentrations of the phases, $\xi = a, \varphi, p, b, m$ for austenite, ferrite, perlite, bainite and martensite correspondingly. The quantities K_0^ξ, K_1^ξ, n, m_1, D_0 are parameters of the model; $\boldsymbol{s}$ is a stress deviator where $\boldsymbol{s} = \boldsymbol{\sigma} - \boldsymbol{I}\,\text{tr}\,\boldsymbol{\sigma}/3$; $\dot{w}_p$ is the plastic power where $\dot{w}_p = \boldsymbol{\sigma} \cdot \dot{\boldsymbol{\epsilon}}^p$; J_2 is the second invariant of the stress tensor: $J_2 = \boldsymbol{s} \cdot \boldsymbol{s}/2$; λ and c_V are the heat-conduction and specific-heat coefficients; Q is a heat source.

The mechanical meaning of the Bodner–Partom model parameters is clarified in [24, Chap. 1]. The validity of the model application, particularly for the simulation of welding processes was established in numerous publications reviewed in the monograph [2, Chap. 3].

The thermo-structural strain $\boldsymbol{\epsilon}^{\theta\text{ph}}$ is calculated by making use of the specific volume of the phases V_ξ according to the formula [28]

$$\boldsymbol{\epsilon}^{\theta\text{ph}}\left(\theta, \theta_r, C^\xi\right) = \frac{V_\xi(\theta)\,C^\xi(\theta) - V_\xi(\theta_r)\,C^\xi(\theta_r)}{3V_\xi(\theta_r)\,C^\xi(\theta_r)}\,\boldsymbol{I}. \tag{9}$$

Here θ is the current temperature, θ_r is some reference temperature. In the equation, the summation over the repetitive index ξ is supposed.

The temperature dependencies of the specific volumes $V_\xi(\theta_r)$ in m^3/kg normalized by $\theta_r = 20$ °C are taken in the form [28, pp. 16–24]

$$\begin{aligned}
&V_a\left(\theta, C_p\right) \times 10^3 = 0.12282 + 8.56 \times 10^{-6}(\theta - 20) + 2.15 \times 10^{-3} C_p,\\
&V_{\varphi,\,p,\,b}\left(\theta, 20\,^\circ, C_p\right) \times 10^3 = 0.12708 + 5.528 \times 10^{-6}(\theta - 20),\\
&V_m\left(\theta, 20\,^\circ, C_p\right) \times 10^3 = 0.12708 + 4.448 \times 10^{-6}(\theta - 20) + 2.79 \times 10^{-3} C_p,
\end{aligned} \tag{10}$$

where C_p is the percentage of Carbon.

According to the classical theory of discretely growing bodies, the displacements discontinue $\Delta\vec{u}(\vec{x}, t^*)$ at the boundary S_L; at the time t^* two separate deformable bodies are joined. After that, the boundary S_L becomes an interface. With discontinuities $\Delta\vec{u}$, the field of displacements from the initial state is discontinuous, and the strains are incompatible. The key problem regarding the applicability of the standard FEM will be resolved if we describe the growth process in such a manner that the compatibility conditions for the strains will be satisfied. The simplest way to do that is to generate a FEM mesh that will cover both the growing body (roller) and all the layers to be

built up. This mesh (the number of nodes) does not vary during numerical simulation. The properties of the domain occupied by the roller are determined by its material. The domains to be built up are initially endowed with the properties of a void material, which is assumed thermo-elastic with $E = 0, \nu = 0, \alpha = 0$.

The thermal properties of the void are the same as those of the built-up layers. Hence, the element is void only from a mechanical point of view. During filling, which is a process developing with time, the void elements of the FE mesh are replaced by a melt. It is good to bear in mind that the filling process deforms both the FE mesh covering the roller and the adjacent void elements.

Let a void element $\Delta V\ (t^*)$ having a strain ϵ_{ij}^* be filled with a melt of temperature θ^* at the time t^*. It is assumed that the material of the layer to be built up is stress-free prior to contact with the roller surface:

$$\sigma_{rr} = \sigma_{\varphi\varphi} = \sigma_{zz} = \sigma_{rz} = 0 \quad \text{at } t = t^*. \tag{11}$$

Since the building-up process implies filling up an element with prestrain ϵ_{ij}^* with a material of temperature θ^*, the conditions (11) mean that

$$\sigma_{ij}\left(\epsilon_{kl}^*, \theta^*\right) = 0 \quad \text{in } \Delta V\left(t^*\right). \tag{12}$$

According to (12), the values ε_{ij}^* and θ^* can be treated as eigenstrain and temperature.

It is assumed that the inelastic strain of an element of a layer built up at $t = t^*$ is equal to zero, i.e., $\epsilon_{ij}^p\ (t^*) = 0$ in $\Delta V\ (t^*)$.

For the constitutive equations of the built-up material to be consistent with condition (12), it is sufficient to modify Hooke's law and the initial conditions for the inelastic strains and the parameter of isotropic hardening as follows:

$$\boldsymbol{s} = 2G_f\left(\boldsymbol{e} - \boldsymbol{\epsilon}^p - \boldsymbol{e}^*\right), \quad \operatorname{tr}\boldsymbol{\sigma} = 3K_f \operatorname{tr}\left(\boldsymbol{\epsilon} - \boldsymbol{\epsilon}^* - \boldsymbol{\epsilon}^{\theta \mathrm{ph}}\right), \tag{13}$$

$$\boldsymbol{\epsilon}^p\left(t^*\right) = 0, \quad K\left(t^*\right) = 0. \tag{14}$$

where the subscript "f" refers to the built-up layers. Equations (7) and (8) are the same for built-up materials. With such an approach, the field of additional strains ϵ_{ij} of the build-up elements will be compatible and can be calculated by the standard FEM.

3 Calculation of phase concentrations

A CCT diagram for steel 34CrMo4 is shown schematically in Fig. 2. The horizontal axis corresponds to the relative time $\tau = t - t_a$, where t_a is the time moment when the cooling curve reaches the temperature $\theta = A_{C1} = 790\,^{\circ}\mathrm{C}$ at the beginning of the austenite phase transformation. Thick solid lines bound the regions of phase transformation (RPT): *A–F* denoting austenite to ferrite; *A–P* denoting austenite to perlite; *A–B* denoting austenite to bainite; *A–M* denoting austenite to martensite. Thin solid lines correspond to the experimental cooling trajectories (thermo-kinetic trajectories—TKT). An arbitrary cooling trajectory is shown by the dashed line. The percentage of the ferritic $p_{\varphi e}$, perlitic p_{pe} and bainitic p_{be} phases at the exit point from correspondent RPT along the TKT is marked by numbers.

The law of the new phase p_ξ accumulation along the segment of TKT inside the RPT (except *A–M*) is approximated by the expression [29]

$$p_\xi = \left[1 - \exp\left(-k\frac{\theta_s - \theta}{\theta_s - \theta_e}\right)\right] p_{\xi e}, \quad p_\xi = C^\xi \times 100\%, \tag{15}$$

where k is chosen to be equal to 3; θ_s and θ_e are temperatures at the start and completion of the transformation; $p_{\xi e}$ is the maximum value of the new phase for the current trajectory.

It is assumed [29,30] the phase transformations occur only if the points of the cooling curve are located inside the RPT as long as the real cooling trajectories, being monotonic, differ slightly from the TKT.

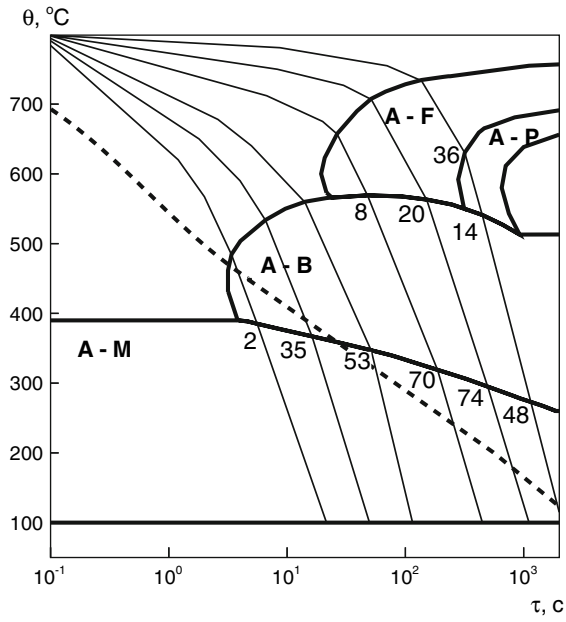

Fig. 2 CCT diagram (scheme)

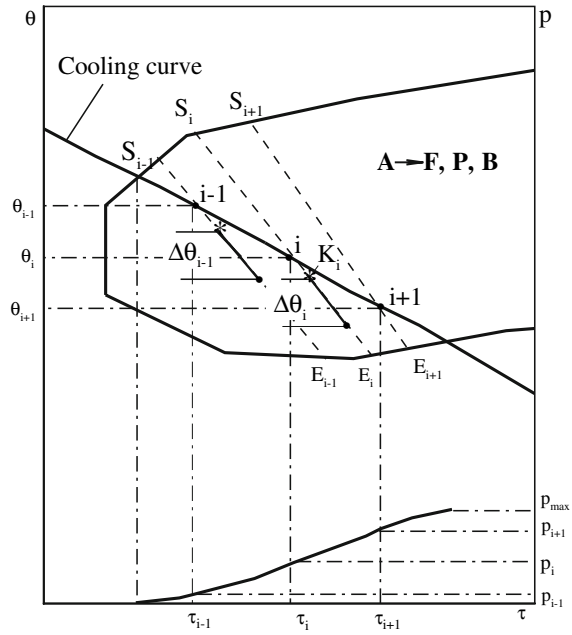

Fig. 3 Scheme of phase calculation

The technique of the phase calculation is based upon the next assumption: the new phase percentage is determined by the formula

$$p_\xi = p_{as} y_\xi, \tag{16}$$

where p_{as} is the austenite percentage upon entering the RPT and $y_\xi = p_\xi / p_{as}$ is the current value of the relative phase. The value of y_ξ is determined by use of the corresponding TKTs; the law of accumulation of the relative phase is similar to the law (15):

$$y_\xi = \left[1 - \exp\left(-k \frac{\theta_s - \theta}{\theta_s - \theta_e}\right)\right] y_{\xi e}. \tag{17}$$

Here $y_{\xi e}$ is the percentage of the new phase at the RPT exit point divided by the percentage of austenite at the entering point.

The cooling process is divided into steps of duration $\Delta\tau_i$. At the first entering of the cooling curve point to the RPT, the value of the austenitic phase p_{as} is fixed.

The phase calculation is illustrated in Fig. 3. At each i^{th} step in time, the point $K_i(\hat{\tau}, \hat{\theta})$ is located on the generated i^{th} trajectory which corresponds to the relative phase y_{i-1} (points with caps). In the vicinity of this point, the increment of the relative phase y is determined by

$$\Delta y_i = (y_{ie} - y_{i-1}) \frac{k|\Delta\theta_i|}{\theta_{si} - \theta_{ei}}. \tag{18}$$

Here $\Delta\theta_i = \theta_i - \theta_{i-1}$.

Then, the phase at the i^{th} point is calculated as

$$p_i = p_{i-1} + p_{as} \Delta y_i. \tag{19}$$

The growth of the martensite phase inside the RPT of *A–M* is determined by the law (15). Also, the temperature at the completion of transformation is the same for all cooling trajectories $\theta_e = 100\,^\circ\text{C}$, and the final value of the martensitic phase p_{me} is equal to the residual percentage of austenite after all other transformations:

$$p_{me} = 100 - p_\varphi - p_p - p_b. \tag{20}$$

The temperature at the transformation start θ_s is determined by the cooling curve entering point to the region of martensitic transformation. In particular, $\theta_s = 390\,^{\circ}\mathrm{C}$ for small transformation times, $\tau \leq 6\,\mathrm{s}$, and θ_s of the martensitic region coincides with θ_s of the bainitic region for $\tau > 6\,\mathrm{s}$.

4 Material properties

The thermomechanical properties of the base material of the roller and the deposited layers are determined by making use of a tensile stress–strain diagram on some strain-rate interval $5 \times 10^{-4}\ \mathrm{s}^{-1} < \dot{\epsilon} < 0.3\,\mathrm{s}^{-1}$ and different temperatures [1, Sect. 1–4].

Experimental data processing results in the calculation of the Bodner–Partom model parameters shown in the Tables 1–3.

To simplify the calculations, it was assumed that the parameter values from Tables 1–3 and the thermal characteristics for all phases are the same. The value $D_0 = 10^4\,\mathrm{s}^{-1}$ has been chosen. CCT diagrams for the steels 34CrMo4 and X30Cr13 were taken from [25, Applications].

5 Solution technique

The problem is solved using a finite-element technique [9,31] based on the approach developed in [32, Chap. 10]. Quadrilateral eight-node isoparametric finite elements were used. The initial FEM mesh and time step were refined to reach 1% of relative accuracy of stress and inelastic strain intensities.

6 Numerical results for austenitic deposited material

In the procedure of gradual growing, beads overlap in each layer (Fig. 1b). To reduce the amount of computation, the number of beads in each layer is restricted to ten. The computations have revealed that end effects localize within

Table 1 Parameters of Bodner–Partom model for steel 34CrMo4

θ, °C	20	400	600	800
n	1.20	1.03	0.80	0.50
m_1, MPa^{-1}	0.15	0.50	1.00	10.0
K_0, MPa	3720.0	3620.0	3200.0	2200.0
K_1, MPa	5520.0	5320.0	4400.0	2700.0

Table 2 Parameters of Bodner–Partom model for steel X30Cr13

θ, °C	20	400	600	800
n	1.05	1.00	0.90	0.54
m_1, MPa^{-1}	0.16	0.20	0.80	10.0
K_0, MPa	1350.0	1200.0	900.0	650.0
K_1, MPa	2450.0	2300.0	1800.0	1300.0

Table 3 Parameters of Bodner–Partom model for steel X5CrNi18-10

θ, °C	20	400	600	800
n	1.05	0.93	0.90	0.85
m_1, MPa^{-1}	0.043	0.12	0.155	0.24
K_0, MPa	1360.0	1220.0	1050.0	1030.0
K_1, MPa	2100.0	1200.0	1190.0	1100.0

the first and last three beads. Hence, the region between the third and seventh beads is that in which a residual stress–strain state holds. This state may be associated with the regular state of the major portion of the roller with completely built-up layers.

The stress–strain state is described by the following invariant characteristics: the intensity of stress deviator s_i, the intensity of the inelastic strains e_i^p, and the mean normal stress:

$$s_i^2 = \frac{1}{6}\left[\left(\sigma_{zz} - \sigma_{\varphi\varphi}\right)^2 + \left(\sigma_{rr} - \sigma_{\varphi\varphi}\right)^2 + (\sigma_{zz} - \sigma_{rr})^2 + 6\sigma_{rz}^2\right], \tag{21}$$

$$\epsilon_i^{p\,2} = \frac{1}{6}\left[\left(\epsilon_{zz}^p - \epsilon_{\varphi\varphi}^p\right)^2 + \left(\epsilon_{rr}^p - \epsilon_{\varphi\varphi}^p\right)^2 + \left(\epsilon_{zz}^p - \epsilon_{rr}^p\right)^2 + 6\epsilon_{rz}^{p\,2}\right], \tag{22}$$

$$\sigma_0 = \frac{1}{3}\left(\sigma_{rr} + \sigma_{zz} + \sigma_{\varphi\varphi}\right). \tag{23}$$

In addition, we use the stress components σ_{zz} and $\sigma_{\varphi\varphi}$ as parameters responsible for brittle fracture. They coincide with the principal normal stresses near the stress-free cylindrical surface. The quantity s_i is responsible for plastic processes and ductile failure. The mean stress identifies the states of tension ($\sigma_0 > 0$) and compression ($\sigma_0 < 0$).

7 Stress–strain state of the first layer

The residual stress–strain state of a roller made of steel 34CrMo covered by two layers of austenitic steel X5CrNi18-4 is considered. The cross-section of the roller is shown in Fig. 1b. The roller geometry is defined by $R = 0.063\,\text{m}$, $L = 0.250\,\text{m}$. The thicknesses of all layers are the same and equal to $0.26 \times 10^{-2}\,\text{m}$. The initial temperature of the roller is $\theta_0 = 300°\text{C}$.

Figure 4 shows the distribution of s_i (curve 1), σ_0 (curve 2), and e_i^p (curve 3) along the line A–A ($r = 0.064\,\text{m}$) going through half the thickness of the first layer cooled down to 20°C . In the A–A section, the interfaces between the beads are shifted to the left by $\sim 0.7\,\text{mm}$ relative to the coordinate z of the bead interface on the roller surface. In the middle region (between the third and seventh beads), the distribution is regularly oscillating with mean values $\bar{s}_i = (\max s_i + \min s_i)/2 = 220\,\text{MPa}$ and $\bar{\sigma}_0 = 245\,\text{MPa}$ and ranges $\Delta s_i = \max s_i - \min s_i < 5.0\,\text{MPa}$ and $\Delta\sigma_0 = 45\,\text{MPa}$. The mean stresses are positive ($\bar{\sigma}_0 > 0$); hence, the built-up layer is in a state of tension, which is typical of built-up austenitic steels. In each bead, the stress σ_0 is maximum (minimum) in the region adjacent to the interface with the bead built up earlier (later). It is near the bead built up earlier where the stresses vary most strongly. In this region, the molten material of the new bead is applied onto the bead built up earlier and already cooled down. The stress intensities s_i have poorly defined maxima near the interfaces. The same place is occupied by the maxima of the residual strains.

The distributions are similar in the case of partial cooling to 300°C. The stress levels are less by about 15% and the maximum residual strains are less by almost 40%.

Assessing the results in terms of coating strength, we conclude that the probability of brittle and ductile failure is higher at the bead interfaces. The maxima σ_{zz} and $\sigma_{\varphi\varphi}$, which coincide with the principal stresses in the surface layers, are very close. This means that, if the built-up layer is mechanically homogeneous and isotropic, a rectangular network of cracks may form, consisting of circumferential cracks initiated by the axial stresses σ_{zz} and longitudinal cracks initiated by the circumferential stresses $\sigma_{\varphi\varphi}$.

8 Stress–strain state of the second layer

Figure 5 shows the distribution of the residual stresses and strains in the second layer cooled down to 20°C over the middle surface B–B ($r = 0.0663\,\text{m}$). In the cross-section B–B, the bead interfaces are shifted to the left by

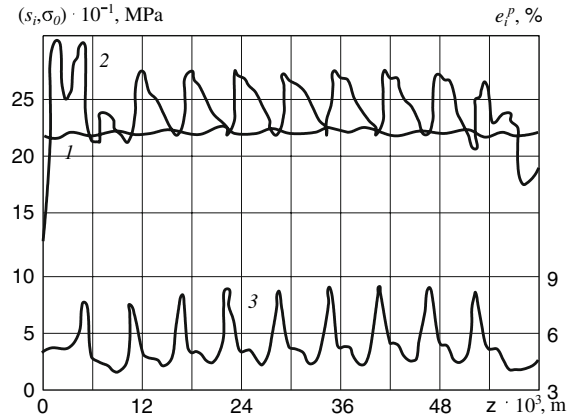

Fig. 4 Distribution of s_i (curve 1), σ_0 (curve 2), and e_i^p (curve 3) along the line A–A

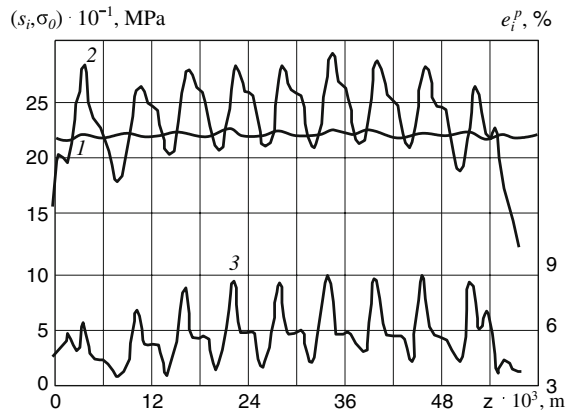

Fig. 5 Distribution of the residual stresses and strains in the second layer cooled down to 20°C over the middle surface B–B

~ 2.0 mm relative to the coordinate z of the interfaces on the roller surface. Curves 1, 2, and 3 correspond to s_i σ_0, and e_i^p, respectively. It is seen that the stress intensity, the mean stress, and the residual strains in the second layer are close to those in the first layer. In the second layer, the maximum of σ_0 is also reached near the interface with the bead built up earlier. The axial component σ_{zz} is the same as in the first layer ($\sigma_{zz} \approx 390$ MPa), and the range is much less. The maximum circumferential stresses are $\sigma_{\varphi\varphi} \approx 440$ MPa. They are larger by 13% than those in the first layer and are reached at the mid-beads.

In the second layer, as in the first one, the regions near the bead interfaces are most prone to brittle and ductile failure. In the case of brittle fracture, cracks are initiated by the circumferential and axial stresses and are oriented in the axial and circumferential directions, respectively. When two and more layers are built up, the above conclusions also apply to the outer layer.

9 Comparison of numerical and experimental data

Let us compare our numerical results with the experimental data obtained by the hole-drilling method [33,34] at the Institute of Welding in Gliwice, Poland. The experimental-theoretical study was conducted for the sixth bead in two layers built up without overlapping (Fig. 1). To measure the residual stresses, a hole 0.0016 m in diameter was drilled to a depth $\delta r = 0.0022$ m at the center of the bead located in the section $z = 0.0304$ m.

It is more convenient to compare the radial stress distributions. According to the experimental procedure, the following stresses are measured and, hence, should be compared with the corresponding theoretical stresses:

$$\sigma_{\min} = \left\langle \min\left(\sigma_{zz}(r),\ \sigma_{\varphi\varphi}(r)\right)\right\rangle_{\delta r}, \qquad \sigma_{\max} = \left\langle \max\left(\sigma_{zz}(r),\ \sigma_{\varphi\varphi}(r)\right)\right\rangle_{\delta r}. \tag{24}$$

where $\langle f(r)\rangle_{\delta r}$ denotes a quantity averaged over the depth of the hole,

$$\langle f(r)\rangle_{\delta r} = \frac{2}{r_0^2 - (r_0 - \Delta r)^2} \int_{r_0-\delta r}^{r_0} f(r)\, r\,\mathrm{d}r. \tag{25}$$

The solid lines in Fig. 6 represent the theoretical radial distributions of the stresses σ_{zz} (curve 1) and $\sigma_{\varphi\varphi}$ (curve 2). The experimental and calculated depth-average maximum and minimum principal stresses are shown by dashed and dotted lines, respectively. It is seen that the maximum and minimum principal stresses do not correlate with any stress component. For example, the stress $\sigma_{\varphi\varphi}$ is predominant on the surface. In deeper layers, the maximum stress is determined by σ_{zz}.

We have proposed a method for the numerical simulation of thermomechanical processes in spirally growing cylindrical bodies. The method is based on the theory of growing bodies, the so-called Bodner–Partom model, and

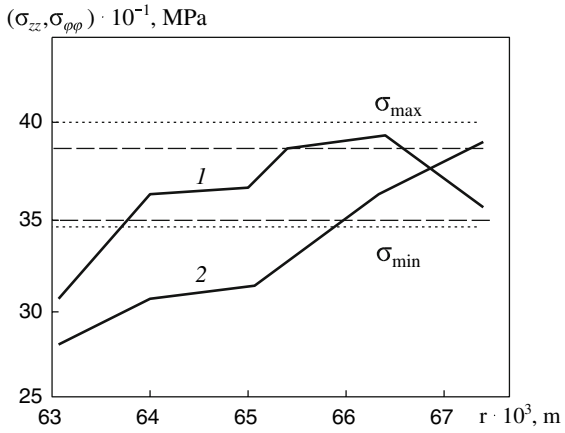

Fig. 6 Radial distributions of the stresses σ_{zz} (curve 1) and $\sigma_{\varphi\varphi}$ (curve 2). The experimental (dashed lines) and calculated (dotted lines) depth-average maximum and minimum principal stresses

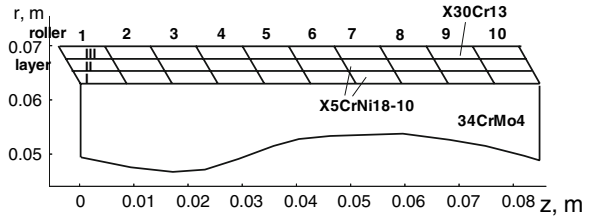

Fig. 7 Roller cross-section

the finite-element method. Residual stresses and strains in a 34CrMo4 steel cylinder with two built-up X5CrNi18-10 steel layers have been calculated. In both layers, the regions in which the beads overlap are most stressed and, thus, most prone to brittle and ductile failure. In the case of brittle fracture, cracks of two types may occur: circumferential cracks, initiated by the axial stresses, and longitudinal cracks, initiated by the circumferential stresses. The theoretical and experimental results are in good agreement.

10 Calculation results for deposited austenitic and martensitic layers

The residual structural and stress states of a roller made of steel 34CrMo4 covered by two layers of austenitic steel X5CrNi18-10 and by one layer of martensitic steel X30Cr13 are considered.

The cross-section of the roller is shown in Fig. 7. It is assumed that the first and second layers retain the austenitic structure. The roller geometry is defined by $R = 0.063$ m, $L = 0.250$ m. The thicknesses of all layers are the same and equal to 0.0026 m. The initial temperature of the roller is $\theta_0 = 300\,^{\circ}$C.

The parameters of heat input are: the electric current is $I = 190$ A; the voltage is $U = 23.6$ V; the velocity of deposition is $v = 0.0067$ m/s; the heat input per unit length is $q = 6.7 \times 10^5$ J/m.

The influence of roller preheating on the phase concentration and maximum principal stress for $\theta_0 = 300\,^{\circ}$C is studied. These data are shown in Figs. 8 and 9. Note that the heat-affected zone (HAZ) of the roller is mainly bainitic while an external layer is martensitic for the most part. Residual distributions of axial and circumferential stresses in the sequences of 1 and 2 shown by thin dashed-point lines in Fig. 8 are presented by solid and dashed lines correspondingly in Fig. 10.

The complicated character of the behavior of the curves is caused by the processes of hardening and structural transformations during layer-by-layer deposition and cooling of metal. As a result of martensite generation in the external layer, the components σ_{zz} and $\sigma_{\varphi\varphi}$ are compressive, while tensile stresses arise in austenitic layers as well as in the near-the-surface part of the roller.

To clarify the influence of the initial temperature on the residual stress and structural states, the case of $\theta_0 = 20\,^{\circ}$C was also considered. It was established that, after the deposition of the first layer, a martensitic HAZ structure is formed. When the second layer has been deposited, the bainite transformation takes place in the near-the-surface part of the roller because the temperature exceeds the transformation value $\theta = A_{C1}$ there. In this case, the martensite phase is conserved in the deeper layer of the roller. This is an indication that the phase concentration control in HAZ is possible through the choice of a suitable value of the preheating temperature. Lower values of preheating temperatures can be used since tempering treatment occurs during the deposition of the following layers [35,36].

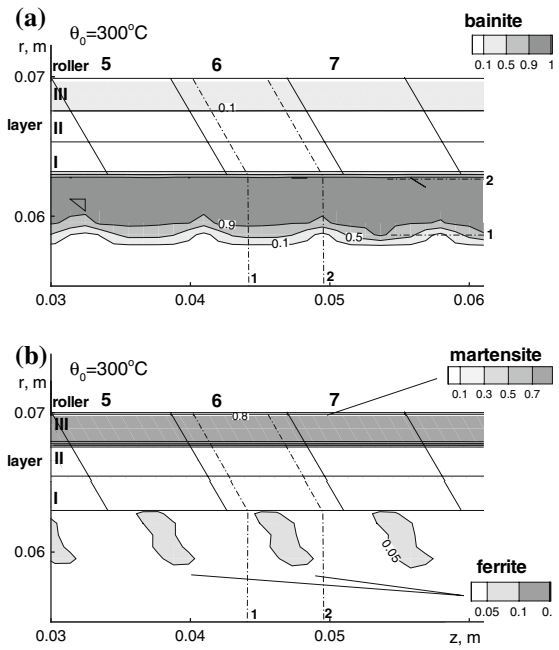

Fig. 8 Concentration of bainite (**a**), and concentrations of martensite and ferrite (**b**) in the surfaced roller for the preheating temperature $\theta = 300°C$

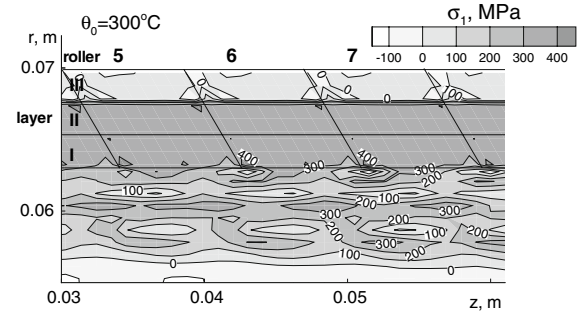

Fig. 9 Maximum normal-stress distribution for $\theta = 300°C$

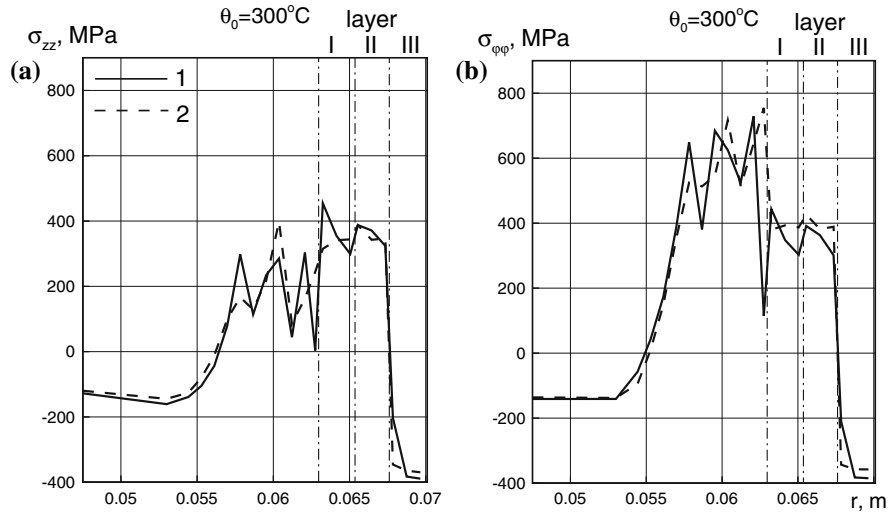

Fig. 10 Radial distributions of axial (**a**) and circumferential (**b**) stresses for $\theta = 300°C$

11 Comparison of theoretical and experimental results

To evaluate the reliability of the calculation technique, a roller made of 34CrMo4 steel with $2R = 0.103$ m and $L = 0.160$ m was surfaced by two X5CrNi18-10 steel layers and then by one X30Cr13 steel layer under typical heat-input conditions. The initial temperature was equal to 200°C.

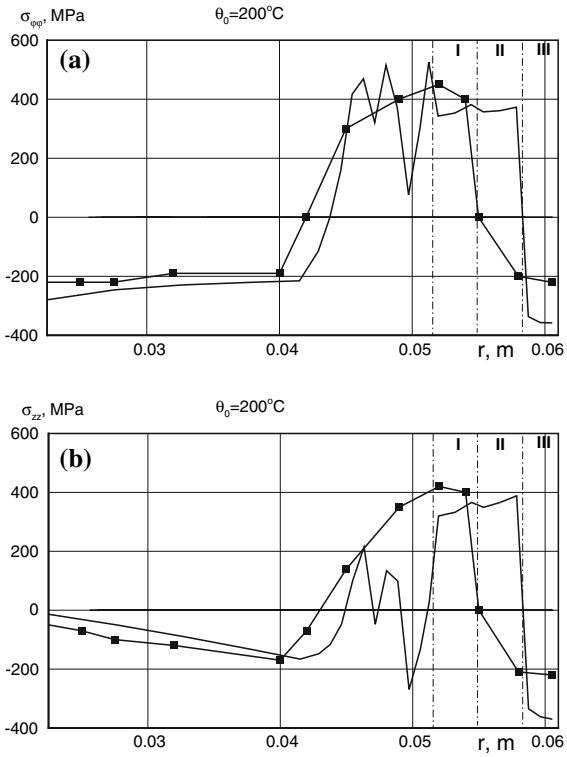

Fig. 11 Comparison of theoretical and experimental distributions of axial σ_{zz} and circumferential $\sigma_{\varphi\varphi}$ stresses

The calculated phase concentration agreed well with experimental data. In particular, mainly a bainite structure of HAZ as well as a martensite structure of the external layer were established. The components of the residual stress were determined by making use of strain-gauge data obtained during a boring measurement in accordance with [37, Chaps. 1–3]. A comparison of calculated and measured stress components σ_{zz} and $\sigma_{\varphi\varphi}$ is presented in Fig. 11.

A satisfactory fit of tension and compression-zone alteration points and levels of the components is observed. Insufficient agreement is observed between the numerical prediction and experimental data particularly in the region $0.04 < r < 0.06$. Firstly, the compressive axial stress $\sigma_{zz} = -210\,\text{MPa}$ is predicted at $r = 0.05\,\text{m}$ while a tensile stress of 370 MPa is measured. Secondly, the values of the measured stresses in the inner layer is somewhat less than the calculated one.

The discrepancies mentioned here are caused by mixing of the roller martensitic steel with the material of the first austenitic layer. As a result, the intermetallic compound does not undergo a deep martensitic transformation or does not undergo a transformation at all.

Similarly, the lower level of the compressive stresses in the inner layer is also the result of partial mixing of austenitic steel of the second layer with the martensitic steel of the inner one. So the martensitic fraction in the intermetallic compound is less than that obtained by simulation. Therefore, the neglect of the mixing processes between austenitic and martensitic materials of the roller and the layers is one of the limitations of the model presented here. Taking account of the mixing is the next possible step to improve the model.

Some discrepancy between the predicted and experimental values is due to mixing of roller and layer materials on the contact surfaces.

12 Conclusions

A new model for determining the current and residual stress–strain and microstructure state of a cylinder subjected to surface-layer deposition by welding has been elaborated. The model is based on the growth-body theory, the

unified Bodner–Partom thermoviscoplastic theory and continuous-cooling transformation diagrams. Unified flow theory operates with total inelastic strain and does not use an explicit flow surface. The Bodner–Partom model is widely used nowadays in static and dynamic thermomechanical problems to model such phenomena as plastic deformation, creep, stress relaxation thermal recovery etc.

Growth theory has been used to describe the essential change of a body during surfacing. To meet the specific boundary conditions on the growth surface, an apparatus of eigenstrains is employed. The developed approach gives the possibility to exclude the disruption of the displacement on the internal surfaces and then to use a standard finite-element technique. Eight-node isoparametric quadrilateral finite elements have been used for the time-step integration of the program.

A method to calculate the microstructure state of a cylinder has been developed. It gives the possibility to determine the microstructure state of an arbitrary material point of a cylinder under cooling by using the change of the austenitic disruption phase along the cooling curves of CCT-diagrams. As an example, the problem of layer surfacing by austenite and martensite steels was considered. Stress and structure residual states were investigated in great detail.

When the roller is surfaced by austenitic steel layers, a residual state of tension ensues. It represents the superposition of some mean and oscillating components varying within the deposited bead. The local maximum of the stress components occurs near the boundary of the previously deposited bead. The bead interfaces are most prone to brittle and ductile failure.

When the roller is being surfaced by austenitic and then martensitic steel layers, the nature of the radial distributions of stress becomes complicated. This is caused by the processes of hardening and structural transformations under layer-by-layer deposition and cooling of the metal. The outer martensitic steel layers are mainly in a martensitic state. But the phase of HAZ is essentially controlled by the initial temperature of the roller and the heat input of deposited layers.

Comparison of numerical and experimental results is fairly good for austenitic layers. Some discrepancy for martensitic layers is caused by neglecting the mixing processes between austenitic and martensitic materials.

References

1. Bezukhov NI, Bazhanov NI, Goldenblat II, Nikolayenko NA, Sinyukov AM (1965) Stress, stability and vibration calculations under high temperatures. Mashinostroeniye, Moscow (In Russian)
2. Radaj D (2003) Welding residual stresses and distortion. Calculation and measurement. DVS Verlag, Dusseldorf
3. Kovalenko VD (1970) Fundamentals of thermoelsticity. Naukova Dumka, Kiev (In Russian)
4. Shevchenko YN (1970) Thermoelasticity under varying loading. Naukova Dumka, Kiev (In Russian)
5. Arutyunyan NH, Drozdov AD, Naumov VE (1987) Mechanics of growing visco-elastoplastic solids. Nauka, Moscow (In Russian)
6. Chromov VN, Senchenkov IK (1999) Hardening and recovery of mashinery components by thermoelastoviscoplastic deformation. OGSHA, Orel (In Russian)
7. Ryabtsev IA (2004) Surfacing of maschine and mechanism components. Ecotechnology, Kiev (In Russian)
8. Paton BE (ed) (1974) Technology of arch welding by melting. Naukova Dumka, Kiev (In Russian)
9. Senchenkov IK, Tabieva GA (2003) Modeling the recondishing of worn-out hollow cylindrical machine parts by thermomechanical deformation. Int Appl Mech 39:110–115
10. Klingbeil NW, Beuth JL, Chin RK, Amon CH (2002) Residual stress-induced warping in direct metal solid freeform fabrication. Int J Mech Sci 44:57–77
11. Tzou HS, Bergman LA (1998) Dynamics and control of distributed systems. Cambridge University Press, Cambridge
12. Zhuk YA, Senchenkov IK (2004) Modelling the stationary vibrations and dissipative heating of thin-walled inelastic elements with piezoactive layers. Int Appl Mech 40:546–556
13. Costescu RM, Cahill DG, Fabriguette FH, Sechrist ZA, George SM (2004) Ultra-low thermal conductivity in W/Al_2O_3 nanolaminates. Science 303:989–990
14. Guz AN, Rushchitskii YY (2003) Nanomaterials: on the mechanics of nanomaterials. Int Appl Mech 39:36–69
15. Ortega AR, Bertram LA, Fuchs EA, Mahin KW, Nelson DV (1993) Thermomechanical modeling of a stationary gas metal arc weld—comparison between numerical and experimental results. Int Trends Weld Sci Technol Material Park, Ohio, ASM International pp. 89–93
16. Troivel L, Nasstrom M, Jonson M (1998) Experimental and numerical study of multi-pass welding process of pipe-flange joints. J Press Vessel Technol (ASME) 120:244–251

17. Zienkevich O, Taylor R (1991) The finite element method, vol 1. McGraw-Hill
18. Nemat-Nasser S (1972) On variational method in finite and incremental elastic deformation problems with discontinuous fields. Q Appl Math 30:143–156
19. Sandhu RS, Salaam V (1976) Variational formulation of linear problems with nonhomogeneous boundary conditions and internal discontinious. Comput Meth Appl Mech Eng 7:75–91
20. Lobanov LM, Sanchenko VA, Pavlovsky VI, Pashchin NA, Senchenkov IK, Chervinko OP, Tabieva GA (1998) Mathematical model for determination of the reciprocal longitudinal displacements of structural members under welding. Avtomaticheskaya svarka 3:5–9 (In Russian)
21. Senchenkov IK, Lobanov LM, Chervinko OP, Pashchin NA (1998) Regularities of relative longitudinal displacements of the aluminium alloy plates under butt welding. Proc Nat Acad Sci Ukraine 6:66–70 (In Russian)
22. Senchenkov IK, Tabieva GA, Ryabtsev IA, Turyk E (2006) Calculation of residual stresses in multilayer helical surfacing of cylindrical components on the basis of the theory of growth of visco-plastic solids. Weld Int 20:150–156
23. Senchenkov IK (2005) Thermomechanical model of growing cylindrical bodies made of physically nonlinear materials. Int Appl Mech 41:1059–1065
24. Bodner SR (2000) Unified plasticity—an engineering approach (Final Report). Faculty of Mech. Eng., Technion
25. Popov AA, Popova AE (1961) The hand-book of the heat-treater. Isothermal and thermo-kinetic diagrams of structural transformation of overcooled austenite. GNTI Mashinostroit. Lit (in Russian)
26. Seyffarth P, Kuscher A (1982) Schweiss-ZTU-Schaubilder. VEB Verlag Technik
27. Senchenkov IK, Zhuk YA, Tabieva GA (1998) Thermodynamically consistent modifications of the generalized thermoviscoplastic models. Int Appl Mech 34:345–351
28. Yuriev SF (1950) Specific volume of phases in the martensitic transformation of austenite. Metallurgizdat (in Russian)
29. Makhnenko VI, Velikoivanenko EA, Kravtsov TG, Sevryukov VV (2001) Numerical investigation of thermomechanical processes under surfacing of rollers of ship devices and mechanisms. Avtomat Svarka 1:3–10 (in Russian)
30. Leblond JB, Mottet G, Devaux JC (1986) A theoretical and numerical approach to the plastic behavior of steel during phase transformation—I Derivation of general relations. J Mech Phys Solids 34:395–409
31. Senchenkov IK, Zhuk YA, Karnaukhov VG (2004) Modeling of thermomechanical behavior of physically nonlinear materials under monoharmonic loading. Int Appl Mech 40:943–969
32. Motovilovets IA, Kozlov VI (1987) Mechanics of coupled fields in the structural members, vol. 1. Thermoelasticity. Naukova Dumka, Kiev (In Russian)
33. Determining of residual stresses by the Hole Drilling gage method. ASTM Standard: E 837
34. Measurement of Residual Stresses by the Hole Drilling Gage Method. Measurements Group Inc. Tech. Note (1993)
35. Dachelean D, Delamarian S (1998) Application of welding for increasing the service life of the power station equipment. Proc of Conference welding and related technologies for the 21st century. Kiev, 78–87
36. Turyk E (2004) Czynniki warunkujace stan naprezen w elementach napawanych. IX Naukowo-Techniczna Krajowa Konferencja Spawalnicza, Miedzyzdrojeh, pp. 197–207
37. Birger IA (1963) Residual stresses. Mashgiz, Moscow